PARL DEFICIENCY IN MOUSE CAUSES COMPLEX III DEFECTS, COENZYME Q DEPLETION, AND LEIGH-LIKE SYNDROME

Marco Spinazzi[a,b,1], Enrico Radaelli[c], Katrien Horré[a,b], Amaia M. Arranz[a,b], Natalia V. Gounko[a,b,d], Patrizia Agostinis[e], Teresa Mendes Maia[f,g,h], Francis Impens[f,g,h], Vanessa Alexandra Morais[i], Guillermo Lopez-Lluch[l], Lutgarde Serneels[a,b], Placido Navas[l], Bart De Strooper[a,b,m,1]

[a] VIB Center for Brain and Disease Research, 3000 Leuven, Belgium. [b] KU Leuven, Department of Neurosciences, 3000 Leuven, Belgium. [c] Comparative Pathology Core, University of Pennsylvania, School of Veterinary Medicine, Department of Pathobiology, Philadelphia 19104-6051, United States. [d] Electron Microscopy Platform & VIB Bio Imaging Core, 3000 Leuven, Belgium. [e] Cell Death Research & Therapy (CDRT) Laboratory, Department for Cellular and Molecular Medicine, KU Leuven University of Leuven, Leuven, Belgium. [f] VIB-UGent Center for Medical Biotechnology, 9000 Ghent, Belgium. [g] VIB Proteomics Core, Albert Baertsoenkaai 3, 9000 Ghent, Belgium. [h] Department for Biomolecular Medicine, Ghent University, 9000 Ghent, Belgium. [i] iMM Instituto de Medicina Molecular, Faculdade de Medicina, Universidade de Lisboa, 1649-028 Lisboa, Portugal. [l] Centro Andaluz de Biología del Desarrollo and CIBERER, Instituto de Salud Carlos III, Universidad Pablo de Olavide-CSIC-JA, Sevilla 41013, Spain. [m] UK Dementia Research Institute, University College London, ION Gower Street, WC1E 6BT London, UK.

Submitted to Proceedings of the National Academy of Sciences of the United States of America

The mitochondrial intramembrane rhomboid protease Parl has been implicated in diverse functions *in vitro*, but its physiological role *in vivo* remains unclear. Here we show that *Parl* ablation in mouse causes a necrotizing encephalomyelopathy similar to Leigh syndrome, a mitochondrial disease characterized by disrupted energy production. Mice with conditional Parl deficiency in the nervous system, but not in muscle, develop a similar phenotype as germline *Parl* knockouts demonstrating the vital role of Parl in neurological homeostasis. Genetic modification of two major Parl substrates, Pink1 and Pgam5, do not modify this severe neurological phenotype. *Parl*$^{-/-}$ brain mitochondria are affected by severe ultrastructural changes, defects in Complex III activity, coenzyme Q biosynthesis, and mitochondrial calcium metabolism. Parl is necessary for the stable expression of Ttc19, required for Complex III activity, and of Coq4, essential in coenzyme Q biosynthesis. Thus, Parl plays a previously overseen constitutive role in the maintenance of the respiratory chain in the nervous system, and its deficiency causes progressive mitochondrial dysfunction, structural abnormalities leading to neuronal necrosis and Leigh-like syndrome.

rhomboid protease | mitochondria | neurodegeneration | respiratory chain | Leigh syndrome

INTRODUCTION

PARL represents the only known mitochondrial member of the rhomboid family (1). Rhomboids are evolutionary conserved intramembrane cleaving proteases and pseudo proteases involved in a variety of functions (2). Their broad biological significance is reflected in their pathological relevance for prevalent human diseases, including cancer and neurodegenerative diseases (2).

The crucial role of PARL in cellular homeostasis is illustrated by the lethal multisystem phenotype of Parl deficient mice (*Parl*$^{-/-}$), associated with muscle atrophy and increased apoptosis in thymus and spleen (3). The faster cytochrome c release and cristae remodeling *in vitro*, and the increased cell death of *Parl*$^{-/-}$ mouse embryonic fibroblasts (MEFs) treated with apoptosis-inducing agents rescued by overexpressed intermembrane space targeted Opa1, led to the proposal that Parl plays a role in cristae remodeling and cytochrome c release during apoptosis. The authors suggested that decreased Opa1 processing by Parl was causative to these apoptotic phenotypes. Later studies identified Oma1 and Yme1l (4) as the proteases cleaving Opa1 and questioned Opa1 as a Parl substrate. More recently, Parl has been implicated in the processing of other substrates in cultured cells (5–10). Two substrates, Pink1 and Pgam5, are of particular interest as they are implicated in Parkinson's disease (11, 12). Both accumulate in *Parl*$^{-/-}$ cells (6–8, 13), but it is unclear whether this accumulation is detrimental (2). A recent elegant cell biology study proposed that PARL exerts pro-apoptotic effects via misprocessing of the mitochondrial Diablo homolog (hereafter Diablo) (10). However, this is difficult to reconcile with the lethality of *Parl*$^{-/-}$ mice and the proposed protective function of Parl (3). Overall, the available data have led to contradictory speculations with regard to the role of Parl in apoptosis (3, 10), mitochondrial function (3, 14), morphology (3, 14, 15), mitophagy (16–18) and claims have not been further substantiated *in vivo*. More importantly, the cause of death of the *Parl*$^{-/-}$ mice, and therefore the physiological role of this protease has remained unresolved. To address these questions, we re-investigated Parl deficient mice. In contrast with our previous report, we find now, in addition to the described phenotypes in peripheral tissues, that Parl deficiency causes a necrotizing encephalomyelopathy closely resembling Leigh syndrome, a human mitochondrial disease caused by impaired respiratory chain defects (19). A simi-

Significance

Parl is a peculiar protease in the inner membrane of mitochondria with important but unclear physiological roles, and with links to Parkinson's disease and diabetes. Most studies, including the original characterization of the *Parl* knockout mouse and others performed *in vitro*, have focused on apoptosis. We show that Parl deficiency in the nervous system alone or in the complete animal causes severe neurodegeneration associated with necrosis resembling the human mitochondrial disease Leigh syndrome. By combining genetic, biochemical, and proteomic approaches, we show that Parl plays an essential physiological role in the nervous system being required for the maintenance of mitochondrial structure and function at the level of Complex III, Coenzyme Q, and calcium metabolism.

Reserved for Publication Footnotes

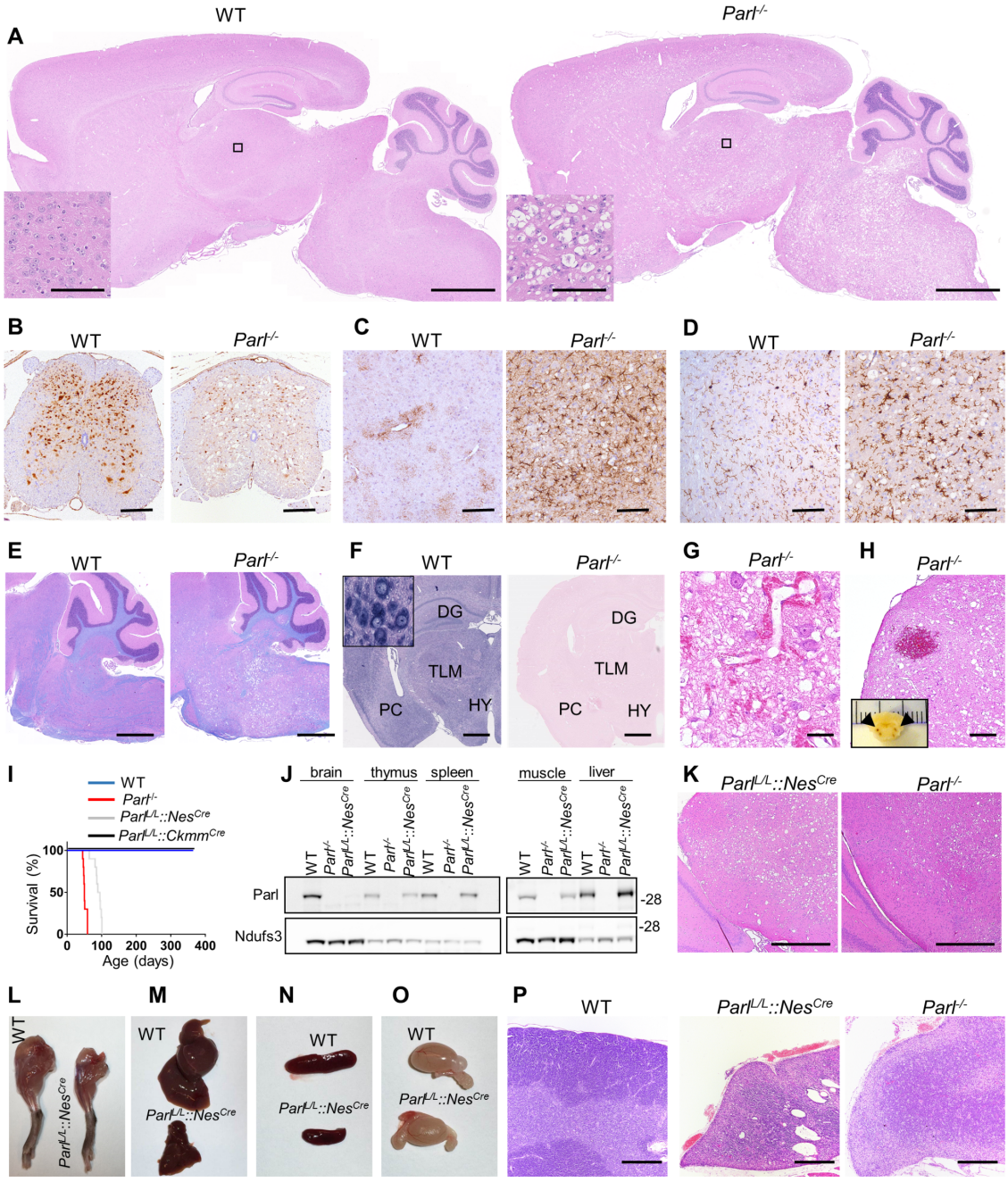

Fig. 1. A Leigh-like encephalomyelopathy drives *Parl*$^{-/-}$ phenotype. (*A*) Severe vacuolar neurodegeneration in a 7 weeks-old *Parl*$^{-/-}$ mouse brain. H&E staining (n≥ 12). Scale bar: 1250 µm. The insert shows a detail of the thalamus (scale bars: 100 µm). (*B*) Severe neuronal loss in the gray matter of *Parl*$^{-/-}$ lumbar spinal cord at 7 weeks of age. NeuN staining (n=3 for WT, n=6 for *Parl*$^{-/-}$). Scale bar: 125 µm. (*C*) Anti-Gfap staining showing prominent astrogliosis in *Parl*$^{-/-}$ medulla oblongata at 7 weeks of age (n=3 for WT, n=6 for *Parl*$^{-/-}$). Scale bar: 125 µm. (*D*) Anti-Iba1 staining in superior colliculus in the midbrain at 7 weeks (n=3 for WT, n=6 for *Parl*$^{-/-}$). Scale bar: 125 µm. (*E*) Combined Luxol fast Blue and H&E staining showing preservation of the white matter (stained in blue) in 7 weeks-old *Parl*$^{-/-}$mice (n=3 for WT, n=7 for *Parl*$^{-/-}$). Scale bar: 750 µm. (*F*)*Parl* in situ hybridization. DG: dentate gyrus; TLM: thalamus; PC: pyriform cortex; HY: hypothalamus. Scale bar: 1 mm. The insert shows strong Parl expression in WT reticular neurons. (*G*) H&E staining of the inferior colliculus in the midbrain of a 7-week old *Parl*$^{-/-}$ mouse showing vascular proliferation (n>10). Scale bar: 50 µm. (*H*) Focal hemorrhage in the olivary nucleus of a 7-week old *Parl*$^{-/-}$ mouse. Bilateral symmetrical hemorrhages have been detected in brainstems of 4 out of 7 *Parl*$^{-/-}$ mice at 7 weeks of age and in none of the WT littermates. Scale bar: 250 µm. The insert shows bilateral symmetrical hemorrhages in medulla oblongata (arrows). (*I*) Survival curves of WT (n=14), *Parl*$^{-/-}$ (n=14), *Parl*$^{L/L}$*::Nes*^{Cre} (n=15) and *Parl*$^{L/L}$*::Ckmm*^{Cre} mice (n=13). (*J*) Western blot analysis of Parl protein in brain, thymus, spleen, muscle, and liver mitochondria isolated from 7 weeks old WT and *Parl*$^{-/-}$, and 13 weeks old *Parl*$^{L/L}$*::Nes*^{Cre}-mice (n=3). Ndufs3 is the loading control. (*K*) H&E staining of midbrains from 10 weeks old *Parl*$^{L/L}$*::Nes*^{Cre} (n=4),and 7 weeks-old *Parl*$^{-/-}$ mice (n=12). Scale bar: 380 µm. (*L-O*) Severe atrophy of the skeletal muscle (*L*), liver (*M*), spleen (*N*) but normal testis size (*O*) in 11-week old *Parl*$^{L/L}$*::Nes*^{Cre}- male mice compared to an age matched WT control (n>15). (*P*)H&E staining of thymus from WT (age: 7 weeks; n=6), *Parl*$^{L/L}$*::Nes*^{Cre} (age 10-13 weeks; n=4), and *Parl*$^{-/-}$ mice (age:7 weeks; n=12). *Parl*$^{L/L}$*::Nes*^{Cre} and *Parl*$^{-/-}$ thymus are atrophic.Scale bar: 200 µm.

lar multisystem phenotype is seen both in the full *Parl*$^{-/-}$ and in *Parl*$^{L/L}$*::Nes*^{Cre} mice with a specific deletion of Parl in the nervous system. The striking neurodegeneration is not associated with altered apoptosis but with massive necrosis raising the question of

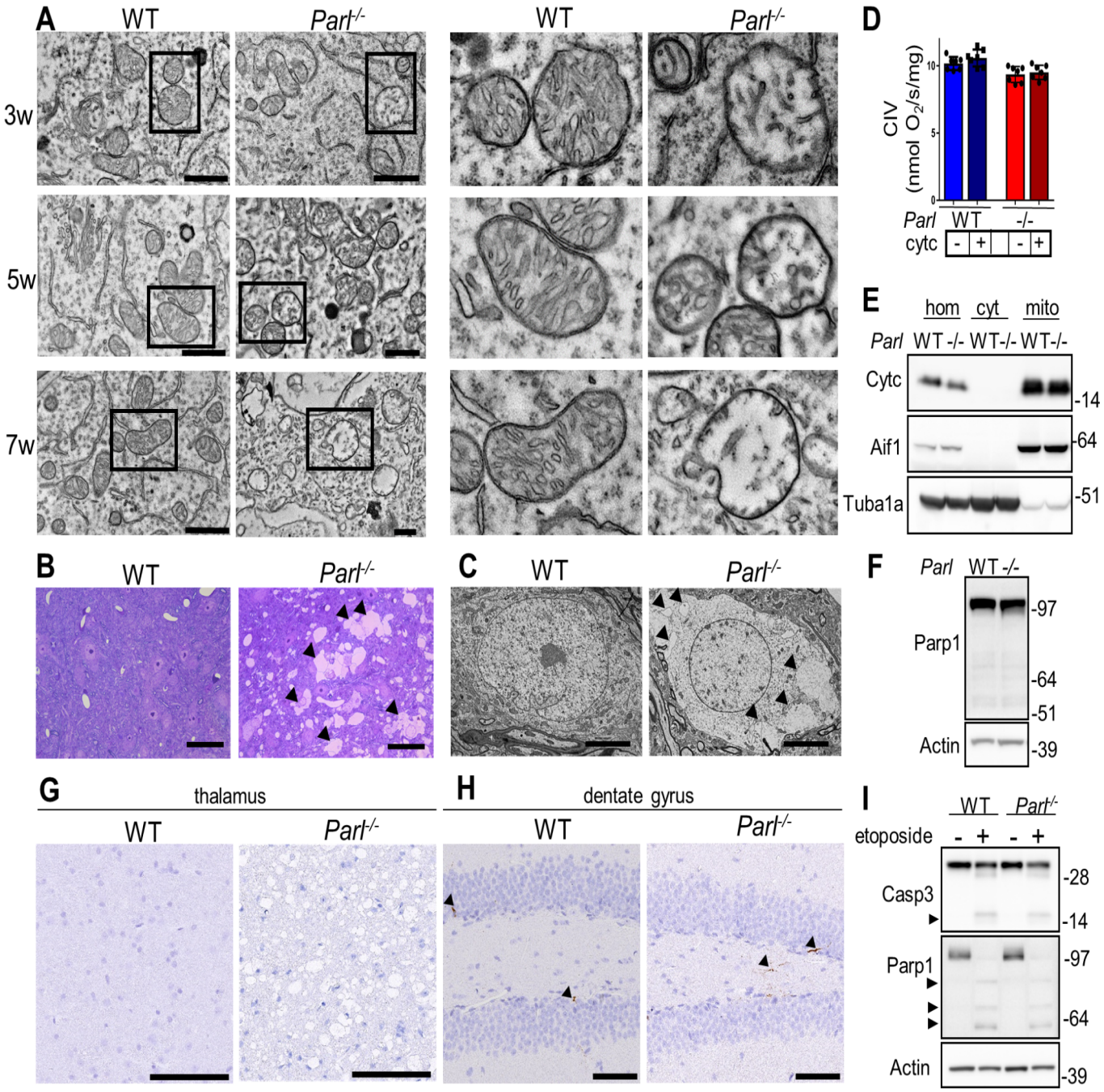

Fig. 2. *Parl*$^{-/-}$ neurodegeneration is preceded by mitochondria ultrastructural changes and is characterized by necrosis. (*A*) Electron microscopy of medulla oblongata neuronal mitochondria of WT and *Parl*$^{-/-}$ over time, at 3, and 7 weeks of age. The right panel represents a high magnification inset of the images shown on the left. Scale bar:1 µm. (*B*) Semithin section stained with toluidine blue shows vacuolization and disintegration of neurons (black arrowheads) in medulla oblongata of 7 weeks old *Parl*$^{-/-}$ mouse compared to a WT. Scale bar: 50µm. (*C*) Representative electron microscopy images showing intracellular vacuolization (black arrowheads) in a 7 week-old *Parl*$^{-/-}$ thalamic neuron. Scale bar: 5µm. (*D*)Permeability of mitochondrial outer membrane by Ascorbate/TMPD-driven oxygen consumption rates in 6 weeks old WTand *Parl*$^{-/-}$ purified free brain mitochondria (n=7) before and after addition of exogenous 10 µM cytochrome c. Data represent average ± SD. (*E*).Western blot of WT and *Parl*$^{-/-}$ brain cytosolic and mitochondrial fractions at 7 weeks of age (n=3) showing absence of cytochrome c into the cytosol. Anti-Aif1 and anti-Tubulin are mitochondrial and cytosolic markers respectively. Hom: total homogenate; cyt: purified cytosol; mito: purified mitochondria. (*F*) Immunoblot of 7 week-old WT and *Parl*$^{-/-}$ nuclei-enriched brain fractions with anti-Parp antibody. (*G*) Activated caspase 3 staining shows absence of positive neurons, in 7 weeks *Parl*$^{-/-}$ thalamus despite the presence of severe neurodegeneration (n=4). Scale bar: 100 µm. (*H*) In the dentate gyrus, a brain area that does not show degeneration in germline or in *Parl*$^{L/L}$::*Nes*^{Cre} mice, activated caspase 3 staining shows scattered positive neurons (black arrows) to the same extent in WT and *Parl*$^{-/-}$ mice (n=4). Scale bar: 50 µm.(*I*)Cultured primary neurons were treated with 10 µM etoposide for 24 hours and lysed. Total neuronal lysates were immunoblotted with anti-Caspase-3 and anti-Parp antibodies. The black arrows indicate the proteolytic fragments of activated caspase 3 and Parp. Actin is the loading control.

the underlying mechanism. We show that necrosis in *Parl*$^{-/-}$ brains is preceded by progressive mitochondrial structural changes and by specific defects of the respiratory chain at the level of Complex III (CIII) and Coenzyme Q (CoQ), and is associated with alter-

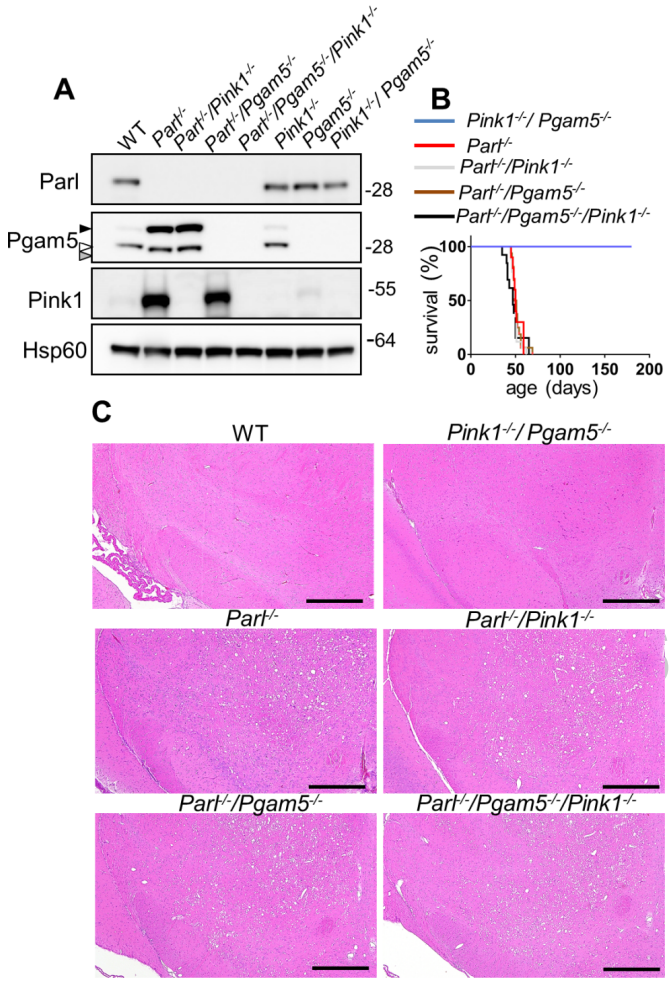

Fig. 3. Pink1 and Pgam5 do not interact genetically with Parl deficiency *in vivo*. (*A*) Validation of *Parl*$^{-/-}$*/Pgam5*$^{-/-}$, *Parl*$^{-/-}$*/Pink1*$^{-/-}$ and *Pink1*$^{-/-}$*/Pgam5*$^{-/-}$ double knockout mice, and *Parl*$^{-/-}$*/Pgam5*$^{-/-}$*/Pink1*$^{-/-}$ triple knockout mice. Brain mitochondria were isolated from mice of the indicated genotype and immunoblotted with Parl, Pink1, and Pgam5 antibodies. The white arrow indicates the mature form of Pgam5, the black arrow indicates the unprocessed form, the grey arrow indicates alternatively processed form in *Parl*$^{-/-}$ mitochondria. Hsp60 is the loading control. (*B*) Survival curves of *Parl*$^{-/-}$ (n=10), *Pink1*$^{-/-}$*Pgam5*$^{-/-}$ (n=10), *Parl*$^{-/-}$*/Pink1*$^{-/-}$ (n=17), *Parl*$^{-/-}$*/Pgam5*$^{-/-}$ (n=16), *Parl*$^{-/-}$*/Pgam5*$^{-/-}$*/Pink1*$^{-/-}$ (n=13). (*C*) H&E staining of midbrain coronal sections of 7 week-old mice of the indicated genotypes (n>3). Scale bar: 500 µm.

ations in mitochondrial calcium metabolism. Thus, Parl has an essential physiological role in the maintenance of mitochondrial structure and function, which is severely impaired when Parl is ablated, causing Leigh-like neurodegeneration. We discuss how these novel insights affect our previous interpretations of the *Parl*$^{-/-}$ phenotype *in vivo*.

RESULTS

Parl deficiency in the nervous system leads to Leigh syndrome

Parl$^{-/-}$ mice develop normally up to the age of 40 days, after which they progressively lose weight (3). From the age of six weeks, they show rapidly progressive locomotor impairment, paresis of the lower limbs, hunchback deformity, and dyspnea (Movie S1). They die before the age of eight weeks from a multisystem phenotype with atrophy of skeletal muscle, thymus and spleen (3), without a clear explanation. Immune deficiency is unlikely the cause of death because thymus and spleen become atrophic only few days before death when mice are already severely affected. Moreover mice are bred in specific pathogen free conditions and do not develop opportunistic infections, leaving open the question of which essential vital function is compromised by Parl deficiency. These clinical signs led us to ask whether this phenotype was caused by neurological involvement. Examination of the brain and spinal cord from *Parl*$^{-/-}$ mice indeed showed a previously overlooked subcortical vacuolar encephalomyelopathy closely resembling Leigh syndrome (Fig. 1*A-H*). Leigh syndrome is a lethal mitochondrial disease characterized by neurological regression and pathologically by vacuolar degeneration and necrosis of the brainstem, basal ganglia and spinal cord, reactive gliosis and vascular proliferation (20). Vacuolization of the neuropil was first detectable in *Parl*$^{-/-}$ mice at five weeks of age, initially circumscribed in the brainstem and in the gray matter of the spinal cord, and then progressively extending anteriorly to hypothalamus, thalamus, deep cerebellar nuclei, and the cingulate cortex. Other areas of the brain, notably most of the cortex, hippocampus and the substantia nigra, were spared. Neuronal loss was detectable by loss of NeuN-positive cells (Fig. 1*B*). Neurodegeneration was accompanied by extensive astrogliosis and microgliosis, indicated by Gfap (Fig. 1*C*) and Iba1 (Fig. 1*D*) immunoreactivity. Luxol-fast blue, a staining used to visualize the white matter, showed comparable reaction in WT and *Parl*$^{-/-}$ mice (Fig. 1*E*). Consistent with neuronal involvement, in situ hybridization shows that *Parl* mRNA expression was particularly abundant in neurons (Fig. 1*F*). In advanced stages, vascular proliferation became evident (Fig. 1*G*), and symmetrical hemorrages were frequently observed at 7 weeks of age in the most severely affected areas of the brainstem and spinal cord (Fig. 1*H*). When Parl was specifically ablated in the nervous system using a Nestin-Cre driver (*Parl*$^{L/L}$*::Nes*^{Cre}) (Fig. 1*J*) a similar lethal phenotype was observed as in the germline *Parl*$^{-/-}$ mice (Fig. 1*I*) including the Leigh-type neuropathology (Fig.1*K*). Apart from a 4-weeks delay in lethality and the absence of testis atrophy (Fig. 1*O*), these mice developed the typical *Parl*$^{-/-}$ multisystem phenotype (3) with severe atrophy of muscle, liver, spleen (Fig.1*L-N*), and thymus (Fig. 1*P*) despite normal Parl expression in these tissues (Fig. 1*J*). To further assess ectopic Cre mediated recombination in these peripheral tissues, we evaluated the presence of recombination by PCR, followed by high-resolution capillary electrophoresis (*SI Appendix*, Fig. *S1A-B*). *Parl*$^{-/-}$ alleles were non-detectable in *Parl*$^{L/L}$*::Nes*^{Cre} spleen and liver, and present to a very low percentage in thymus (2%) and muscle (5%), consistent with the protein data. Thymus and spleen became atrophic in *Parl*$^{L/L}$*::Nes*^{Cre} as in germline *Parl*$^{-/-}$ mice only in preterminal stages of the disease when the mice were already affected by severe neurological deficits. Conversely, deletion of Parl in striated muscle in *Parl*$^{L/L}$*::Ckmm*^{Cre} knockout mice using *Cre* expression driven by the Creatine kinase promoter did not compromise survival at least up to the age of 18 months nor led to overt locomotor deficits (n=13, Fig. 1*I*). Altogether, these data suggest that *Parl* deficiency in the nervous system is sufficient to recapitulate the lethal multisystem phenotype of germline *Parl*$^{-/-}$ mice, except the gonad atrophy.

Parl deficiency causes early neuronal mitochondrial ultrastructural abnormalities followed by neuronal necrosis

To characterize mitochondrial ultrastructure and the morphological features of cell death induced by Parl deficiency in the brain we performed electron microscopy. At 3 weeks of age, which is before the occurrence of clinical signs or histopathological lesions, *Parl*$^{-/-}$ but not WT neurons of medulla oblongata, displayed scattered swollen mitochondria with abnormal cristae and a translucent matrix (Fig.2*A*). At later time points, mitochondrial ultrastructural abnormalities became progressively more severe and diffuse in the context of progressive neuronal vacuolization, swelling and loss of integrity (Fig. 2*B-C*). This picture is indicative of necrosis, while the typical morphological signs of apoptosis

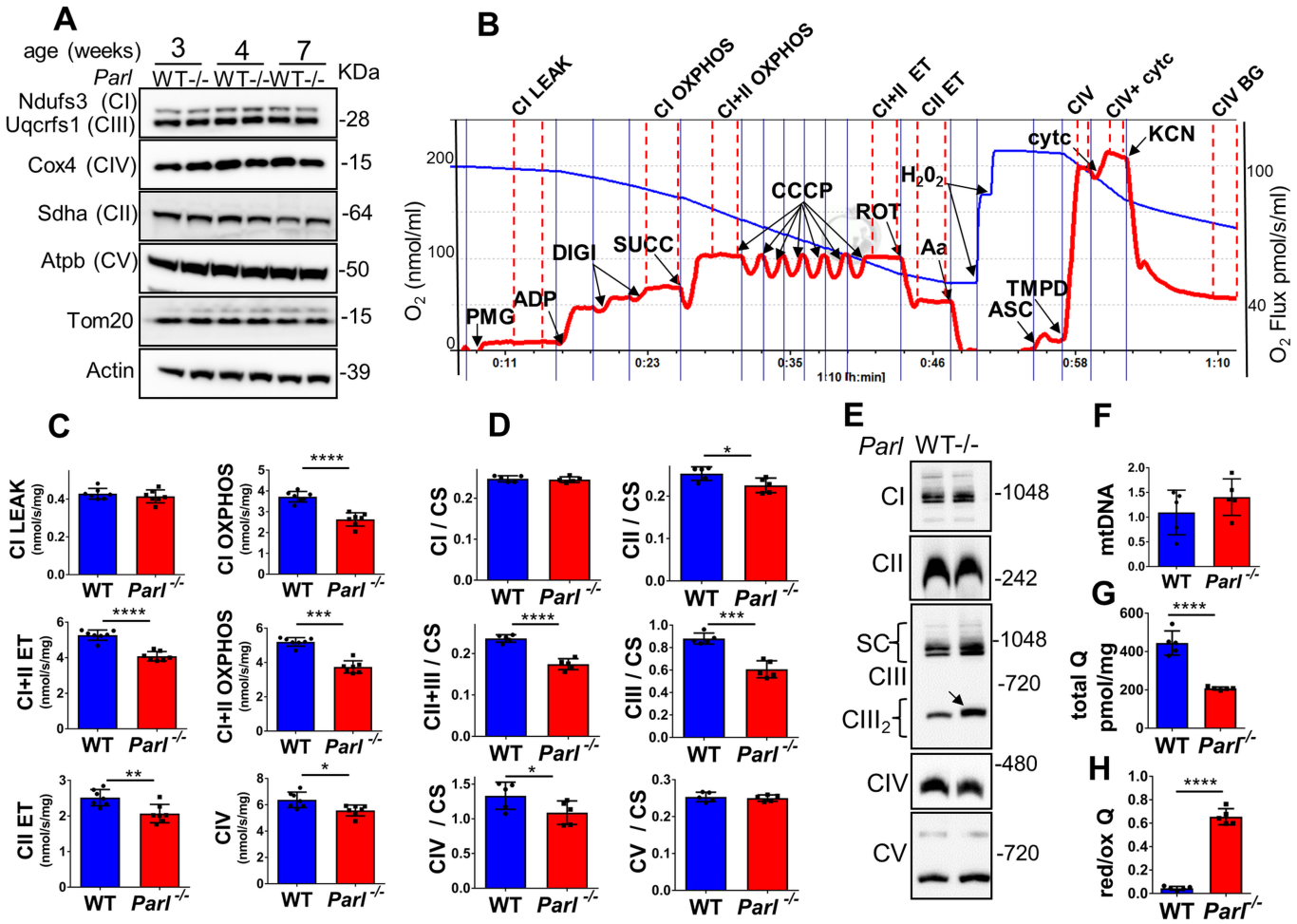

Fig. 4. Defects in CIII and CoQ in *Parl*$^{-/-}$ brain mitochondria. (*A*) Immunoblot of mitochondrial respiratory chain subunits (CI-CV), Tom20, in WT and *Parl*$^{-/-}$ whole brain lysates at 3, 4, and 7 weeks of age (n=4). Actin is the loading control. (*B*)Representative trace illustrating the protocol for high-resolution respirometry in neuronal mitochondria. The blue trace indicates the O_2 concentration, the red trace indicates its time derivative. 50 µg purified synaptosomes were loaded in Miro6 buffer. Digitonin (Digi) was titrated to achieve optimal synaptosomal permeabilization. Substrates: CI (PMG=pyruvate+malate+glutamate), CII (Succ=succinate); CIV (ASC/TMPD=ascorbate+TMPD). Uncoupler: CCCP. Inhibitors: CI (ROT: rotenone); CIII (Aa: Antimycin a); CIV (KCN: potassium cyanide). Cyt c: cytochrome c. Respiratory states are indicated between red dashed lines. CI LEAK=CI-driven leak respiration. CI OXPHOS: CI-driven phosphorylating respiration. CI+II OXPHOS: phosphorylating respiration driven by combined activation of CI and II. CI+II ET: electron transfer capacity driven by combined CI and II. CII ET: electron transfer driven by CII. CIV: CIV-driven respiration. Cytc: exogenous cytochrome c is added to evaluate the integrity of the outer mitochondrial membranes. H_2O_2 in the presence of catalase is used to reoxygenate the chamber. (*C*)Quantification of the respiratory states of permeabilized synaptosomes isolated from six-weeks old WT and *Parl*$^{-/-}$ mice (n=7) as from the protocol in C. (*D*)Enzymatic activities of individual respiratory chain complexes and CII+III in brain mitochondria from 6 weeks old WT and *Parl*$^{-/-}$ mice (n=5) normalized to citrate synthase. (*E*)Blue-native-gel electrophoresis of purified brain mitochondria from 7 weeks old WT and *Parl*$^{-/-}$ mice, followed by immunoblotting with anti-Ndufs3 (CI), anti-Sdha (CII), anti-Uqcrfs1 (CIII), anti-Cox4 (CIV), anti-Atpb (CV). The arrow indicates the upward mobility change of $CIII_2$ in *Parl*$^{-/-}$ (n=3). (*F*) Mitochondrial DNA, normalized by nuclear DNA in 7 weeks old WT and *Parl*$^{-/-}$ brainstems (n=5). (*G*) Concentration of total CoQ (Q_9+Q_{10}) measured by HPLC in brain tissue from 7 weeks old WT and *Parl*$^{-/-}$ mice (n=5).(*H*)Ratio between reduced and oxidized CoQ from the experiment in G. The bar graphs indicate the average ± SD. Statistical significance has been calculated by two sided student t test: *= p<0,05; **=p<0,01; ***=p<0,001;****=p<0,0001.

were consistently absent. Similar abnormalities were present in neuronal mitochondria from *Parl*$^{L/L}$::*Nes*^{Cre} mice (*SI Appendix*, Fig.S2). Since Parl has been linked previously to apoptosis (3, 10) we investigated further its contribution to the neurodegeneration. During apoptosis, the outer mitochondrial membrane becomes permeable, and cytochrome c is released from the mitochondrial intermembrane space to the cytosol leading to proteolytic activation of executioner caspases and Parp. We analyzed mitochondrial outer membrane permeability of brain mitochondria isolated from symptomatic *Parl*$^{-/-}$ mice by measuring the enhancement of Complex IV-driven (CIV) respiration before and after addition of exogenous cytochrome c, which is unable to reach CIV if outer membranes are intact. Exogenous cytochrome c did not significantly enhance CIV-driven respiration in both WT and *Parl*$^{-/-}$ brain mitochondria (Fig. 2*D*), indicating intactness of outer mitochondrial membranes even in advanced stages of the disease with severe neurodegeneration. Consistently, cytochrome c was undetectable in purified brain cytosols from *Parl*$^{-/-}$ brains (Fig. 2*E*), and the expression of full length Parp was similar in *Parl*$^{-/-}$ and WT brains without evidence of proteolytic activation (Fig. 2*F*). Accordingly, we did not see TUNEL-positive cells in the degenerating brain areas, notably brainstem, thalamus, hypothalamus at serial time points ranging from asymptomatic to late stage of the disease (*SI Appendix*, Fig. S3*A*). TUNEL-positivity was restricted to few scattered cells undergoing developmental apoptosis in periventricular areas not affected by *Parl*$^{-/-}$ neurodegeneration. This was not more severe in *Parl*$^{-/-}$ than in WT brains. We obtained similar results using antibodies against cleaved caspase 3 in both

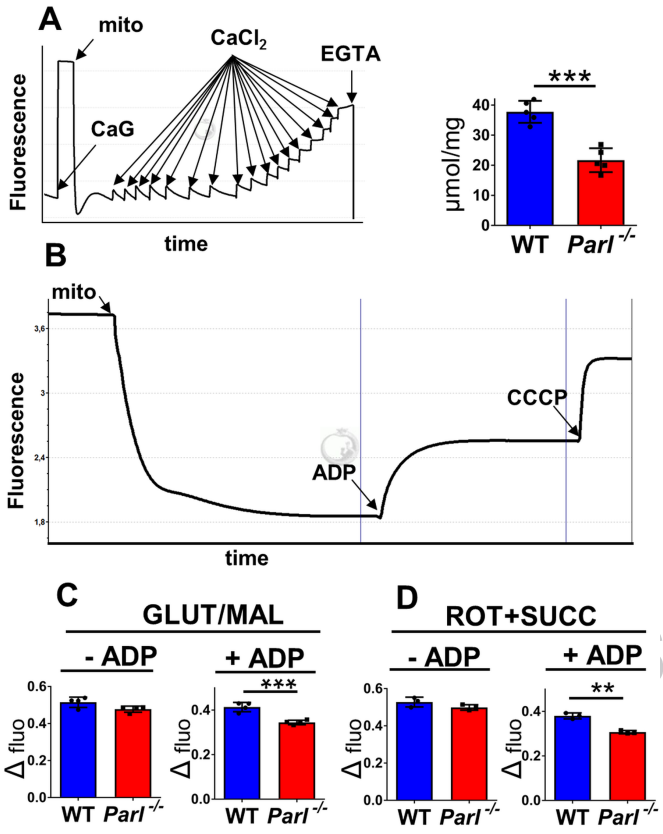

Fig. 5. Alterations in calcium uptake and membrane potential in *Parl*$^{-/-}$ brain mitochondria.(*A*) Calcium retaining capacity of purified brain mitochondria. On the left a representative trace of a typical fluorimetric experiment using Calcium Green illustrating the protocol detailed in methods section. Mito=mitochondria; CaG=Calcium Green; $CaCl_2$=calcium chloride titrations.. EGTA=calcium chelator. On the right the graph bars represent the quantifications of the maximal amount of exogenous calcium retained by WT and *Parl*$^{-/-}$ brain mitochondria purified from 6 weeks old mice before observing calcium efflux (n=5). (*B*) Mitochondrial membrane potential (Δψ) in brain mitochondria using safranin. A typical fluorimetric experiment illustrating the protocol detailed in the method section. Mito=mitochondria; CCCP=uncoupler. (*C-D*) Quantifications of the experiments described in A using exactly 150 µg brain mitochondria from 7 weeks old WT and *Parl*$^{-/-}$ mice (n=5 in C, n=4 for in D). (*C*) Δψ using the CI substrates glutamate and malate (GLUT/MAL) without (leak state) and with ADP (phosphorylating state). (*D*) Δψ using the CII substrate succinate in presence of the CI inhibitor rotenone without (leak state) and with ADP (phosphorylating state). The graph bars indicate the average ± SD. Statistical significances by two-sided t test: **=p<0.005; ***=p<0.0005

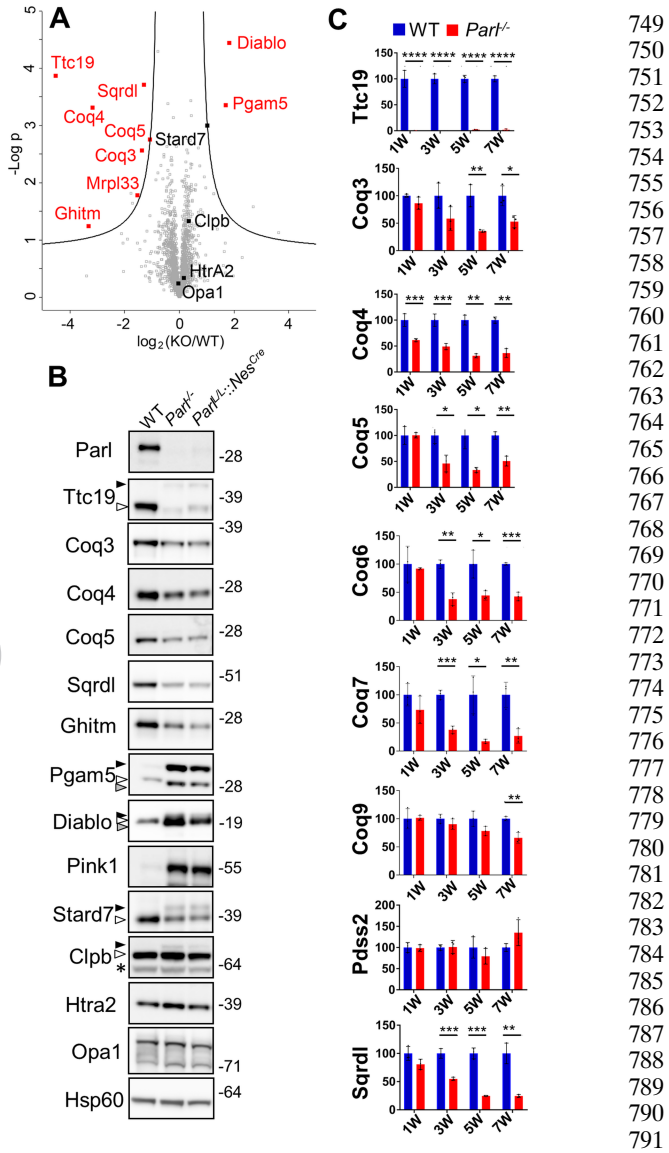

Fig. 6. Restricted changes in the brain mitochondrial proteome induced by Parl deficiency explain the CIII and CoQ defects. (*A*)Volcano plot showing differentially regulated proteins in *Parl*$^{-/-}$ brain mitochondria purified from 5 week-old WT and *Parl*$^{-/-}$brains (n=3) analyzed by mass spectrometry. Significantly differentially regulated proteins are distributed outside the volcano cutoff of fold changes >2 and p value <0.05. Differentially expressed mitochondrial proteins are plotted in red. Previously reported Parl substrates that did not reach statistical significance are plotted in black. The non-mitochondrial proteins Trabd, Bcap31, Bcan, Eif1a, and Setdb, were not included in the graph since appeared similarly expressed in the validation experiment in Fig.6*B*. (*B*)Validation of the mass spectrometry results and of previously reported Parl substrates Pink1, Stard7, Clpb, Htra2, Opa1. Brain mitochondria isolated from WT, *Parl*$^{-/-}$, and *Parl*$^{L/L}$*::Nes*^{Cre}, were analyzed by immunoblotting. The white arrows indicate the mature (processed) form of the protein, the black arrows indicate unprocessed forms, the grey arrows indicate alternatively processed forms in *Parl*$^{-/-}$mitochondria. The asterisk indicates bands of uncertain significance. (*C*)Time course of Ttc19, CoQ biosynthesis proteins and Sqrdl in WT and *Parl*$^{-/-}$brains. Total brain lysates from WT, *Parl*$^{-/-}$ sacrificed at 1, 3, 5, and 7 weeks of age (n=3), were analyzed by immunoblotting (original blots in *SI Appendix,* Fig.S8). The graph bars indicate the quantifications. Each protein was normalized with the loading control Hsp60 and expressed as % relative to the WT. .

Parl$^{-/-}$ (Fig.2*G-H*) and in *Parl*$^{L/L}$*::Nes*^{Cre} mice (*SI Appendix,* Fig. S3*B*), indicating that apoptosis is not overtly altered in Parl deficient brains. Conversely, active Caspase 3 immunostaining of atrophic thymus of severely affected *Parl*$^{-/-}$ mice showed strong positivity (*SI Appendix*, Fig. S3*C*) as previously reported (3). However, an identical thymus pathology (Fig. 1*P*) and caspase-positivity (Fig.S3C) were also seen in late stage *Parl*$^{L/L}$*::Nes*^{Cre} despite normal Parl expression in this tissue (Fig. 1J) indicating that this phenotype can be fully induced by deficiency of Parl in the nervous system alone. Treatment of primary cultures of *Parl*$^{-/-}$ and WT neurons with the pro-apoptotic drug etoposide showed similar proteolytic activation of Caspase 3 and Parp indicating that apoptosis execution is not overtly blocked in cultured neurons (Fig. 2*I*). All together, these data indicate that the striking neurodegeneration induced by Parl deficiency is preceded by mitochondrial ultrastructural abnormalities that accumulate with time. The neurodegeneration is characterized by neuronal necrosis without overtly altering apoptosis. The increased apoptosis in *Parl*$^{-/-}$ immune organs is indirect.

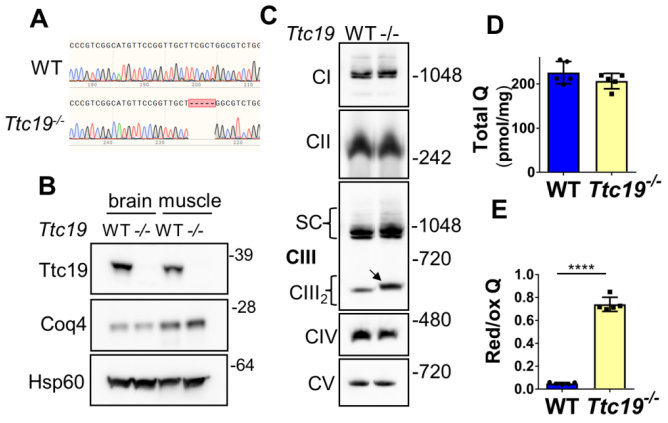

Fig. 7. Ttc19 deficiency causes alterations in CIII and CoQ red/ox but non in CoQ concentration in the nervous system. (*A*)Generation of *Ttc19*$^{-/-}$ mice by Crisper/Cas9 technology. *Ttc19*$^{-/-}$ mice have a 5 base pairs deletion in the first exon. (*B*) Immunoblot analysis of brain and muscle mitochondria with anti Ttc19 and anti Coq4 antibodies. Hsp60 is the loading control. (*C*) Blue-native gel-electrophoresis of purified brain mitochondria from 7 weeks old WT and *Ttc19*$^{-/-}$mice, followed by immunoblotting with anti-Ndufs3 (CI), anti-Sdha (CII), anti-Uqcrfs1 (CIII), anti-Cox4 (CIV), anti-Atpb (CV). The arrow indicates the upward mobility change of $CIII_2$ in *Ttc19*$^{-/-}$ mitochondria. (*D*) Concentration of total CoQ Q (Q_9+Q_{10}) in brains from 7 weeks old WT and *Ttc19*$^{-/-}$mice (n=5). (*E*)Ratio between reduced and oxidized CoQ from the experiment in D. The bar graphs indicate the average ± SD. Statistical significance has been calculated by two sided student t test: ****=p<0,0001.

Parl$^{-/-}$ Leigh-like syndrome is not caused by misprocessing of Pink1 and Pgam5

Next we wondered to what extent the neurodegenerative phenotype of *Parl*$^{-/-}$ mice can be attributed to misprocessing of the best characterized substrates of Parl, Pink1 (16, 6, 8), a mitochondrial kinase, and Pgam5, a mitochondrial phosphatase (9). Both have roles in neurological diseases (11, 12) and in mitophagy (12, 21). Pgam5 has also been linked to regulation of multiple cell death pathways including necroptosis (22). However, the contribution of Pink1 and Pgam5 misprocessing to the *Parl*$^{-/-}$ phenotype is not known (1). Expression of Lc3, p62, and Bnip3 (Figure S4*A*), which are markers of macroautophagy, and mitochondrial protein ubiquitination (Figure S4*B*), which labels proteins of dysfunctional mitochondrial for degradation by mitophagy, were not modified in *Parl*$^{-/-}$ brains, indicating unaltered steady state levels of autophagy in *Parl*$^{-/-}$ brain. Pink1 was barely detectable in WT mitochondria, while a remarkable accumulation of Pink1 was seen in *Parl*$^{-/-}$ brain mitochondria (Fig. 3*A*). Similarly, the unprocessed full-length form of Pgam5 strongly accumulated in *Parl*$^{-/-}$ mitochondria while the processed form of Pgam5 migrated slightly faster than in WT mitochondria, indicating an alternative Parl-independent cleavage. To test whether accumulation of these unprocessed forms of Pink1 and Pgam5 in *Parl*$^{-/-}$ mitochondria drives *Parl*$^{-/-}$ neurodegeneration, we generated a series of double *Parl*$^{-/-}$/*Pink1*$^{-/-}$, *Parl*$^{-/-}$/*Pgam5*$^{-/-}$, and triple *Parl*$^{-/-}$/*Pink1*$^{-/-}$/*Pgam5*$^{-/-}$ combined knockout mice (Fig.3*A*). Surprisingly, the *Parl*$^{-/-}$ phenotype was unmodified by simultaneous deletion of Pink1, or Pgam5, either alone or together, and all these mouse strains invariably died at a similar age as the single *Parl*$^{-/-}$ (Fig.3*B*) affected by similar Leigh-like syndrome (Fig.3*C*). To test whether deficient proteolytic products of Pink1 and Pgam5 generated by Parl were essential, we also generated *Pink1*$^{-/-}$/*Pgam5*$^{-/-}$mice. Conversely, *Pink1*$^{-/-}$/*Pgam5*$^{-/-}$ mice had a normal lifespan (Fig. 3*B*) beyond the age of two years without any overt clinical or neuropathological phenotype (Fig. 3*C*) indicating that misprocessing of Pink1 and Pgam5 alone or together do not explain the *Parl*$^{-/-}$ associated Leigh-like syndrome

Parl deficiency leads to severe respiratory chain defects converging on Complex III and Coenzyme Q

Leigh syndrome is caused by different genetic defects that ultimately impair mitochondrial energy production (19). Therefore, we evaluated how brain mitochondrial function is compromised by absent Parl expression. Since Parl has been previously linked to differences in mitochondrial biogenesis (14), we asked whether mitochondrial mass is affected in *Parl*$^{-/-}$ brains. Expression of respiratory chain subunits and of the outer membraner protein Tomm20 was similar in WT and *Parl*$^{-/-}$ brains at any age (Fig. 4*A*), indicating unaltered mitochondrial mass. Mitochondrial DNA abundance was also not significantly different (Fig. 4*F*). Next, we measured oxygen consumption rates in neuronal mitochondria derived from permeabilized synaptosomes by high-resolution respirometry supplying consecutively substrates and specific inhibitors for CI, II, and IV as illustrated in Fig. 4*B*. Importantly, at three weeks of age, which is three weeks before the first clinical signs of *Parl*$^{-/-}$ mice, respiration was comparable between WT and *Parl*$^{-/-}$ brain mitochondria (*SI Appendix*, Fig. S5*A*). However, at six weeks of age, at the onset of the symptomatic stage, both ADP stimulated respiration (OXPHOS), reflecting the maximal capacity to generate ATP, and uncoupled respiration, providing an estimate of the maximal electron transfer capacity (ET), were severely diminished in *Parl*$^{-/-}$ neuronal mitochondria (Fig. 4*C*). Oxygen consumption was similarly decreased when using only CI substrates (CI OXPHOS), or CI and II substrates simultaneously in both phosphorylating and uncoupled states (CI+II OXPHOS and ET). Respiration from cytochrome c oxidase (CIV) was slightly, although significantly compromised (Fig. 4*C*). To localize precisely the respiratory chain defect, we measured the maximal enzymatic activities of each Complex (CI-CIV) and of ATP synthase in brain mitochondria, as well as the coupled enzymatic activity of CII+III. This enzymatic assay explores segment CII-coenzyme Q-CIII. We detected a severe enzymatic defect of CIII and of CII+III (Fig. 4*D*), while CII and IV activities were slightly, although still significantly, decreased. Next, we wondered whether the deficient CIII activity was due to abnormal CIII assembly. Blue-native-gel electrophoresis of brain mitochondria showed effective assembly and maturation of the four respiratory chain CI-IV and of ATP synthase, as well as preserved formation of the super complex (Fig. 4*E*). The terminal component of CIII, Uqcrfs1, was normally incorporated, but $CIII_2$ showed consistently a slightly lower electrophoretic mobility in *Parl*$^{-/-}$ compared to WT mitochondria (Fig. 4*E*). An identical $CIII_2$ migration abnormality has been recently reported in mitochondria deficient of Ttc19 (23) and gene mutations in *TTC19* cause human Leigh syndrome (24). Next to investigate unambiguously the possibility of CoQ deficiency, we directly measured CoQ levels (CoQ_{9+10}) in brain extracts and the ratio between reduced and oxidized CoQ, a sensitive marker of the electron transfer efficiency (25). CoQ deficiency is one of the established causes of Leigh syndrome (19). Remarkably, total CoQ levels were severely decreased in *Parl*$^{-/-}$ brains at 7 weeks of age (Fig. 4*G*). Moreover, the ratio between reduced and oxidized forms of CoQ was strongly increased (Fig. 4*H*) indicating a marked impairment in $CoQH_2$ oxidation, consistent with the impaired CIII activity. These changes were in contrast to the respiration defect, already severe at the presymptomatic age of 3 weeks (*SI Appendix,* Fig.S5B) indicating that CoQ deficiency is an early effect of Parl deficiency. In conclusion, Parl is required to prevent severe alterations in the respiratory chain of brain mitochondria characterized by CIII and CoQ biosynthesis defects.

Altered calcium metabolism, membrane potential, and reactive oxygen species production in *Parl*$^{-/-}$ brain mitochondria

Next we wondered whether Parl deficiency compromises other important mitochondrial functions in brain mitochondria.

Increased production of reactive oxygen species (ROS) is a possible consequence of respiratory chain defects. Therefore, we measured ROS production rates in brain mitochondria supplemented with both CI and II substrates fluorometry with the H_2O_2 sensor Amplex Ultrared as illustrated in *SI Appendix,* Fig.S6*A*. ROS production was similar in all experimental conditions except for a slight increase only with CI substrates (*SI Appendix,* Fig.S6*B*). Consistently, protein carbonylation, a commonly used biomarker to assess oxidative stress *ex vivo*, was not overtly increased in *Parl*$^{-/-}$ brain mitochondria or total homogenates compared to WT (*SI Appendix,* Fig.S6C-D).

Mitochondrial calcium is an important determinant of cell death and is bi-directionally related to energy metabolism. Both excessive levels of mitochondrial calcium and reduced buffering of cytosolic calcium can be detrimental (26). Therefore, we measured the maximal calcium retention capacity in purified brain mitochondria progressively loaded with calcium (Fig 5*A*, left). *Parl*$^{-/-}$ brain mitochondria showed a severely reduced calcium capacity (Fig 5*A*, right). To investigate whether this defect could be explained by mitochondrial depolarization, we measured the mitochondrial potential ($\Delta\psi$) in brain mitochondria supplied with CI and CII substrates in the absence and in the presence of ADP (Fig 5*B*). In this experiment, $\Delta\psi$ is inversely related to the fluorescence of safranin which is quenched in the mitochondrial matrix of polarized mitochondria. As expected, the addition of ADP consistently led to increased fluorescence, corresponding to a drop in $\Delta\psi$ which reflects the use of the proton gradient to drive ATP synthesis, and the mitochondrial uncoupler CCCP led to a further increase. $\Delta\psi$ in *Parl*$^{-/-}$ brain mitochondria was diminished only in presence of ADP (in phosphorylating conditions), by using both CI and II substrates (Fig. 5*C-D*, right), while the maximal $\Delta\psi$ measured in the absence of ADP was unaltered (Fig. 5*C-D,* left). Therefore, the decreased mitochondrial calcium uptake, which is evaluated in the leak state in the absence of ADP, is not simply explained by mitochondrial depolarization. In conclusion, Parl deficiency leads to severe alterations of mitochondrial calcium metabolism and to modest changes in oxidative stress in the brain.

Mitochondrial proteome changes induced by Parl deficieny in the brain

We wondered what mitochondrial protein changes underlie the observed CIII and CoQ defects in *Parl*$^{-/-}$ brains. We performed a mass spectrometry-based proteome analysis of brain mitochondria purified from WT and *Parl*$^{-/-}$ mice, leading to the quantification of 781 out of 1085 proteins annotated in the mouse mitochondrial proteome in Swissprot (Table S1). The volcano plot showed that despite the dramatic phenotype, surprisingly few mitochondrial proteins were differentially expressed (Fig. 6*A*), indicating selective effects of Parl on the mitochondrial proteome. Among these, we found a striking downregulation of the CIII regulating protein Ttc19 (23, 27) and of several proteins required for CoQ biosynthesis (Coq3, Coq4, Coq5). We also noticed the significant decrease of the sulfide-CoQ oxidoreductase, which has been recently reported to decrease in human primary CoQ defects (28). Ghitm, a multipass inner membrane protein not previously linked to Parl, in contrast, decreased. Like Pink1 and Pgam5, also Diablo (10) increased in Parl deficient brain mitochondria (Fig. 6A). Next, we validated these findings by western blot in brain mitochondria from WT, *Parl*$^{-/-}$, and *Parl*$^{L/L}$*::Nes*^{Cre} (Fig. 6*B*). Since our proteomic approach identifies substrates by expression changes, we decided to include in the validation also the previously reported Parl substrates Htra2 (5), Opa1 (3), Stard7, and Clpb (10), which were not significantly different in our mass spectrometry analysis despite being covered (Fig. 6*A*). Western blots confirmed the virtual disappearance of Ttc19, a marked reduction of the CoQ proteins (Coq3,Coq4,Coq5), Sqrdl, and Ghitm, and altered cleavage of Ttc19, Pgam5, Diablo, Stard7, and Clpb. The expression and processing of Htra2 and Opa1 were not impaired (Fig. 6*B*). To correlate these protein changes with the clinical phenotype, we checked their expression in brain tissue over time, at the age of 1, 3, and 5 weeks, when *Parl*$^{-/-}$ mice are still asymptomatic, and at 7 weeks, when the mice are severely affected by neurological deficits (Fig. 6*C*, *SI Appendix* Fig. S7).

To further investigate the molecular basis of the CIII and CoQ deficiency we included in this time course an extensive panel of proteins required for CoQ biosynthesis (Fig 6C and *SI Appendix* Fig. S8). The virtual disappearance of mature Ttc19 in *Parl*$^{-/-}$ brains at all ages indicates that Parl is required for Ttc19 maturation and expression. Coq4 was also reduced in *Parl*$^{-/-}$ brains already at 1 week of age (Fig. 6*C* and *SI Appendix* Fig. S8), followed by decreased Coq3, Coq5, Coq6, Coq7, Coq9 and of Sqrdl at later time points. Other proteins already affected at the age of one week are Ghitm and Stard7 in addition to Pink1 and Pgam5, while Diablo accumulated only in late symptomatic stages (*SI Appendix* Fig. S7). Expression of Clpb, Htra2, and Opa1 was largely unaffected by Parl expression at all ages, except for a tendency for increased expression of the short Opa1 isoform at 7 weeks of age (*SI Appendix* Fig. S7).

To explore to what extent the catalytic function of Parl is involved in these protein changes, we checked the expression of these proteins in stable *Parl*$^{-/-}$ MEFs expressing Parl^{WT} or catalytic inactive Parl^{S275A} (*SI Appendix*, Fig. S9). We observed no altered mobility of Coq4, Coq5, Sqrdl in *Parl*$^{-/-}$ cultured MEFs, suggesting that they likely are not direct Parl substrates. In contrast, the processing of Ttc19, Pink1, Pgam5, Stard7, Diablo, and Clpb was clearly modified by expression of catalytically active Parl, but not by mutant Parl^{S275A}, confirming that Parl proteolytic activity is required for the maturation of these proteins and that they are all likely genuine Parl substrates (10). In contrast, we could again not confirm differences in Htra2 and Opa1 processing in *Parl*$^{-/-}$ MEFs suggesting that both are not Parl substrates in contrast to previous reports (3, 5).

Effects of Parl deficiency on Ttc19 and Coq4 in liver and muscle

To investigate to what extent Parl deficiency also affects expression of Ttc19 and Coq4 in other organs than the brain, we blotted extracts of liver and skeletal muscle from *Parl*$^{-/-}$, *Parl*$^{L/L}$*::Nes*^{Cre} and WT mice (*SI Appendix*, Fig. S10). As in the nervous system, Ttc19 expression was almost absent in both liver and skeletal muscle tissue of. *Parl*$^{-/-}$ mice only. Coq4 was significantly diminished in both tissues, although to a lesser extent in *Parl*$^{-/-}$ muscle compared to brain and liver. Next, we checked CoQ concentrations and red/ox ratio as well as CIII activity in muscle and found altered CIII activity and CoQ red/ox ratio in. *Parl*$^{-/-}$ muscles but normal CoQ concentration. These data indicate that Parl is required for the expression of Ttc19 and Coq4 in different organs *in vivo*, although Parl deficiency in muscle compromises only CIII activity but not CoQ concentration.

Ttc19 deficiency causes CIII defects and altered CoQ red/ox but not altered CoQ biosynthesis

To dissect the relationship between the Ttc19 deficiency and the observed CoQ defects we generated *Ttc19*$^{-/-}$ mice (Fig. 7*A-B*). These mice (20 out of 20) have not shown any reduced survival although they display a slight reduction in locomotor activity at one year of age. Neuropathological analysis of the brainstem of *Ttc19*$^{-/-}$ mice at the age of seven weeks did not demonstrate lesions(*SI Appendix*, Fig. S11), at difference with *Parl*$^{-/-}$ mice. Blue-native-gel electrophoresis of *Ttc19*$^{-/-}$ brain mitochondria showed a similar upward mobility shift of $CIII_2$ as seen with *Parl*$^{-/-}$ mitochondria (Fig. 7*C*). Coq4 expression (Fig. 7*B*) and CoQ concentration (Fig. 7*D*) were normal but the CoQ red/ox ratio was highly increased in *Ttc19*$^{-/-}$ (Fig. 7*E*) as in the *Parl*$^{-/-}$ brains (Fig. 4*H*). Thus, deficiency of mature Ttc19 in *Parl*$^{-/-}$ brains explains the

altered CIII structure and function, but not the CoQ biosynthesis deficit. Altogether, the data indicate that Parl is required for the maintenance of CIII activity by stabilization of Ttc19, and for efficient CoQ biosynthesis in the brain by stabilizing Coq4 expression (*SI Appendix,* Fig.S12*A-B*).

DISCUSSION

This work reveals an essential role of Parl for the homeostasis of the nervous system. Deficiency of Parl in the nervous tissue whether isolated or in the context of systemic Parl knockout, leads to severe neurodegeneration similar to the CI deficient *Ndufs4*$^{-/-}$ mouse (29, 30), the only currently available mouse model for Leigh syndrome. Although caution is needed before extrapolating from mouse to human diseases, the current study prompts to investigate whether *PARL* gene mutations are present in human patients with unexplained Leigh-like syndrome. Deletion of *Parl* in the nervous system alone in *Parl*$^{L/L}$*::Nes*^{Cre} largely mimics the germline *Parl*$^{-/-}$ phenotype, like *Ndufs4*$^{L/L}$*::Nes*^{Cre} recapitulates that of germline *Ndufs4*$^{-/-}$, indicating that in both models the nervous system involvement drives the disease. This observation demonstrates that the Leigh syndrome is the elusive cause of the multisystem lethal phenotype previously decribed in *Parl*$^{-/-}$ mice (3). Interestingly, severe neurological alterations have also been observed in flies carrying mutations in rhomboid-7 (31), the fly orthologue of Parl. Therefore, specific deletion of *Parl* in the nervous system also causes severe atrophy of skeletal muscle, thymus, and spleen as in germline *Parl*$^{-/-}$ mice (6), although with a delay of about one month. Nonspecific Cre recombinase activity driven by Nestin was very limited or undetectable in these tissues and Parl protein expression unaffected, therefore very unlikely contributing to these *Parl*$^{L/L}$*::Nes*^{Cre} phenotypes. Moreover, the lack of overt muscle atrophy and of lethality in mice with specific deletion of *Parl* in muscle, as opposed to the nervous system, indicates that the severe muscle atrophy is mainly a consequence of the neurodegeneration. Brain specific deletion of the mitochondrial protease Htra2 affects thymus and spleen in a similar way as brain specific Parl deficiency (32). Such immunological phenotypes can be caused by a variety of general stress conditions that trigger increased secretion of corticosteroids and other stress hormones which induce apoptosis in these tissues (33). Hind limb unloading for instance induces the distinctive depletion of double positive CD4+CD8+ T lymphocytes that was also observed in *Parl*$^{-/-}$ thymus and a drop of B lymphocytes as was seen in *Parl*$^{-/-}$ spleen (3), but general stress conditions such as malnutrition (34), or neurological diseases (35) can have similar effects on apoptosis in thymus and spleen, at least in mice. This is consistent with the observation that *Parl*$^{-/-}$ and *Parl*$^{L/L}$*::Nes*^{Cre} mice develop these immunological manifestations only in late stages of the neurological disease.

Since the original description of *Parl*$^{-/-}$ mice (3), many studies have focused on possible links between Parl and apoptosis *in vitro* with controversial results (3, 5, 10). Here we were unable to confirm a role of Parl in apoptosis *in vivo* (3), instead we observe a severe necrotic neuronal phenotype. We speculate that the necrotic encephalopathy may represent a tissue specific consequence of the severe structural and functional damage that progressively accumulate in *Parl*$^{-/-}$ neuronal mitochondria, rather than the result of a direct gatekeeping activity of Parl in regulated necrosis machineries. Although we were not able to define in further detail whether necrosis is regulated in *Parl*$^{-/-}$ brains, the neuropathological phenotype is consistent with the definition of Leigh syndrome as a necrotizing encephalomyelopathy.

Surprisingly, despite the striking neuropathology, the absence of Parl affects only a very circumscribed proportion of the brain mitochondrial proteome, which overlaps with recent proteomic data obtained in HEK293 cells (10). One limitation of our proteomic approach is that it only evaluated protein expression but not post-translational modifications and in particular cleavage sites were not analysed. At odd with previous observations (3, 5) and consistent with following reports (10, 36), the data presented here do not support Opa1 and Htra2 as substrates of Parl. Conversely, we find several proteins differentially regulated by Parl deficiency and several of them play important roles in neurological diseases. We tested explicitly whether Pink1 and Pgam5, two substrates of Parl involved in Parkinson's disease (11, 12) and mitophagy (12, 21), could drive the pathological phenotype of *Parl*$^{-/-}$ mice. Rare *PARL* mutations have been reported in rare patients with Parkinsons's Disease (16). We tested combined knockouts of these two substrates with *Parl*$^{-/-}$ and their combined deletion in the presence of Parl to check whether the accumulation or the loss of function of these two substrates would play a role, but none of these experiments modulated or simulated the *Parl*$^{-/-}$ phenotype. Thus, Pink1 and Pgam5 are not responsible for the Leigh-like pathology in the *Parl*$^{-/-}$ mice indicating that other biochemical mechanisms are involved.

Here we show that Parl plays an essential role in the respiratory chain independently from effects on mitochondrial mass (14) by regulating proteins implicated in CIII and CoQ biogenesis. Parl is required for the expression of Ttc19 (Fig. 6*B-C*) and impaired proteolytic maturation of Ttc19 by Parl likely leads to its degradation by alternative mitochondrial proteases. A recent study reported that Parl is required for Ttc19 cleavage *in vitro* (10) but the functional consequences were not investigated. Ttc19 is involved in the turnover of the iron-sulfur protein Uqcrfs1 (23), a structural subunit of CIII essential for the catalytic activity that ensures CoQ oxidation. Here we show that impaired proteolytic maturation and expression of Ttc19 in *Parl*$^{-/-}$ tissues results in altered CIII structure and catalytic activity as in *Ttc19*$^{-/-}$ mitochondria. The defective CIII activity is reflected by the increased fraction of reduced vs oxidized CoQ. When CIII activity is normal, CoQ red/ox ratio is low, while it is high when CIII is dysfunctional, in both *Parl*$^{-/-}$ and *Ttc19*$^{-/-}$ mice. In addition, and independently from Ttc19, Parl modulates the expression of Coq4, a protein required for the biosynthesis of CoQ (37). Intriguingly, the severe CoQ deficiency that we found in *Parl*$^{-/-}$ brains is followed by a secondary reduction in the expression of Sqrdl, as also recently observed in primary CoQ defects (28). CoQ is a highly hydrophobic molecule functioning as an electron carrier from several metabolic pathways to CIII and as membrane antioxidant (38, 39). The mechanism that links ablation of Parl to the reduced Coq4 and the resulting CoQ deficiency in the brain is however not yet clear, since we could not demonstrate that Coq4 is a substrate of Parl. One possibility is that misprocessing of a still undefined Parl substrate affects CoQ biosynthesis upstream of Coq4, similarly to how the yeast intermediate peptidase Oct1p ensures CoQ biosynthesis by cleaving Coq5p (40). An alternative hypothesis is that Parl regulates CoQ biosynthesis indirectly by generating an early stress response that precedes the respiration defects. Recent observations show that the CoQ pathway is sensitive to different mechanisms affecting mitochondrial DNA gene expression in mouse heart tissue (41). However, in these models Parl expression was upregulated, while Coq4 was unmodified or increased, in contrast with what we observe in *Parl*$^{-/-}$ mice. Thus, the effects caused by Parl deficiency are clearly different from those reported in that study.

The *Ttc19*$^{-/-}$ mice data indicate that the CoQ deficiency is independent from the CIII defect and therefore Parl plays an essential role in the maintenance of the respiratory chain by two distinct mechanisms. Interestingly, human mutations in *TTC19* (24), and in genes that induce CoQ deficiency (19) are independent causes of Leigh syndrome. In addition, *COQ4* haploinsufficiency cause neurodegeneration in human (37). However, deletion of *Ttc19*

in mouse causes only mild neurodegeneration at advanced ages (23), and accordingly we did not observe the massive brainstem encephalopathy in *Ttc19*$^{-/-}$ of *Parl*$^{-/-}$ mice at comparable age (*SI Appendix* Fig. S11). One hypothesis is that the respiratory chain dysfunction determined by the combination of the CIII and CoQ defects drive the *Parl*$^{-/-}$ Leigh-like encephalopathy. This might be a possible explanation for the apparent resistance of the skeletal muscle to Parl ablation, since in this tissue decreased Coq4 is not associated with a significant drop in CoQ concentration, as in the nervous system. However, we cannot exclude that other mitochondrial functional and structural defects caused by Parl deficiency could also contribute to the pathogenesis of the neurodegeneration. We didn't find a major impact of Parl deficiency in oxidative stress in the brain but we found that Parl deficiency has severe consequences on mitochondrial calcium metabolism. Mitochondrial calcium is a critical determinant of cell death including necrosis and is particularly important in neurodegenerative disorders including Parkinson's, amyotrophic lateral sclerosis, Huntington disease (26), and hereditary neurodegenerative diseases caused by mutations in another mitochondrial protease, *AFG3L2* (42). Moreover, mitochondrial function is bidirectionally related to mitochondrial structure, and we found that *Parl*$^{-/-}$ brain mitochondria progressive accumulate morphological abnormalities implying that Parl plays a role, whether direct or indirect, in mitochondrial ultrastructure. It is thus plausible that the drastic neurodegeneration that we report in *Parl*$^{-/-}$ mice is due to a combination of mitochondrial functional and structural defects that progressively accumulate culminating in neuronal necrosis.

Our work indicates that Parl has a constitutive physiological role in keeping mitochondrial function and structural integrity in check, with crucial consequences for the nervous system.

MATERIALS AND METHODS

Details are provided in *SI Appendix*, *SI Materials and Methods*, including details on mice, pathology, ISH, electron microscopy, subcellular fractionation, Immunoblot, BNGE, high-resolution respirometry, mitochondrial respiratory chain enzyme CoQ, ROS production, protein carbonylation, mitochondrial calcium, antibodies, proteomics, plasmids, mtDNA quantifications, cell culture, statistics.

ACKNOWLEDGEMENTS

This work was supported by Fonds voor Wetenschappelijk Onderzoek, Methusalem grant, Geneeskundige Stichting Koningin Elisabeth, Bax-Vanluffelen, "Opening the Future" , Vlaams Initiatief voor Netwerken voor Dementie Onderzoek (VIND), Spanish Ministry of Health, FIS PI17-01286 grant. Hercules Type 1 AKUL/09/037. We thank A. Francis, E. Seuntjens, V.Hendrickx, J.Verwaeren for help. M.S. is recipient of EMBO long-term fellowship (ALTF 648-2013). **AUTHOR CONTRIBUTIONS** M.S. and B.D.S. conceived the project and wrote the paper. M.S. performed and analyzed most of the experiments, with help from all coauthors. All authors reviewed and approved the manuscript. The authors declare no competing interests

1. Spinazzi M, De Strooper B (2016) PARL: The mitochondrial rhomboid protease. *Semin Cell Dev Biol* 60:19–28.
2. Düsterhöft S, Künzel U, Freeman M (2017) Rhomboid proteases in human disease: Mechanisms and future prospects. *Biochim Biophys Acta - Mol Cell Res* (February):0–1.
3. Cipolat S, et al. (2006) Mitochondrial Rhomboid PARL Regulates Cytochrome c Release during Apoptosis via OPA1-Dependent Cristae Remodeling. *Cell* 126(1):163–175.
4. Anand R, et al. (2014) The i-AAA protease YME1L and OMA1 cleave OPA1 to balance mitochondrial fusion and fission. *J Cell Biol* 204(6):919–929.
5. Chao J-R, et al. (2008) Hax1-mediated processing of HtrA2 by Parl allows survival of lymphocytes and neurons. *Nature* 452(7183):98–102.
6. Deas E, et al. (2011) PINK1 cleavage at position A103 by the mitochondrial protease PARL. *Hum Mol Genet* 20(5):867–879.
7. Jin SM, et al. (2010) Mitochondrial membrane potential regulates PINK1 import and proteolytic destabilization by PARL. *J Cell Biol* 191(5):933–942.
8. Meissner C, Lorenz H, Weihofen A, Selkoe DJ, Lemberg MK (2011) The mitochondrial intramembrane protease PARL cleaves human Pink1 to regulate Pink1 trafficking. *J Neurochem* 117(5):856–867.
9. Sekine S, et al. (2012) Rhomboid protease PARL mediates the mitochondrial membrane potential loss-induced cleavage of PGAM5. *J Biol Chem* 287(41):34635–34645.
10. Saita S, et al. (2017) PARL mediates Smac proteolytic maturation in mitochondria to promote apoptosis. *Nat Cell Biol* 19(4):318–328.
11. Valente EM, et al. (2004) Hereditary Early-Onset Parkinson ' s Disease Caused by Mutations in PINK1. *Science (80-)* 304(May):1158–1161.
12. Lu W, et al. (2014) Genetic deficiency of the mitochondrial protein PGAM5 causes a Parkinson's-like movement disorder. *Nat Commun* 5:4930.
13. Greene AW, et al. (2012) Mitochondrial processing peptidase regulates PINK1 processing, import and Parkin recruitment. *EMBO Rep* 13(4):378–385.
14. Civitarese AE, et al. (2010) Regulation of skeletal muscle oxidative capacity and insulin signaling by the mitochondrial rhomboid protease PARL. *Cell metab* 11(5):412–426.
15. Jeyaraju D V, et al. (2006) Phosphorylation and cleavage of presenilin-associated rhomboid-like protein (PARL) promotes changes in mitochondrial morphology. *Proc Natl Acad Sci U S A* 103(49):18562–18567.
16. Shi G, et al. (2011) Functional alteration of PARL contributes to mitochondrial dysregulation in Parkinson's disease. *Hum Mol Genet* 20(10):1966–1974.
17. Meissner C, Lorenz H, Hehn B, Lemberg MK (2015) Intramembrane protease PARL defines a negative regulator of PINK1- and PARK2/Parkin-dependent mitophagy. *Autophagy* 11(9):1484–1498.
18. Shi G, McQuibban GA (2017) The Mitochondrial Rhomboid Protease PARL Is Regulated by PDK2 to Integrate Mitochondrial Quality Control and Metabolism. *Cell Rep* 18(6):1458–1472.
19. Lake NJ, Compton AG, Rahman S, Thorburn DR (2016) Leigh syndrome: One disorder, more than 75 monogenic causes. *Ann Neurol* 79(2):190–203.
20. Lake NJ, Bird MJ, Isohanni P, Paetau A (2015) Leigh syndrome: neuropathology and pathogenesis. *J Neuropathol Exp Neurol* 74(6):482–92.
21. Yamano K, Youle RJ, Yamano K, Youle RJ (2016) PINK1 is degraded through the N-end rule pathway PINK1 is degraded through the N-end rule pathway. 8627(July). doi:10.4161/auto.24633.
22. Wang Z, Jiang H, Chen S, Du F, Wang X (2012) The mitochondrial phosphatase PGAM5 functions at the convergence point of multiple necrotic death pathways. *Cell* 148(1–2):228–243.
23. Bottani E, et al. (2017) TTC19 Plays a Husbandry Role on UQCRFS1 Turnover in the Biogenesis of Mitochondrial Respiratory Complex III Article TTC19 Plays a Husbandry Role on UQCRFS1 Turnover in the Biogenesis of Mitochondrial Respiratory Complex III. *Mol Cell*:1–10.
24. Koch J, et al. (2015) Mutations in TTC19: Expanding the molecular, clinical and biochemical phenotype. *Orphanet J Rare Dis* 10(1):1–12.
25. Guarás A, et al. (2016) The CoQH2/CoQ Ratio Serves as a Sensor of Respiratory Chain Efficiency. *Cell Rep* 15(1):197–209.
26. Abeti R, Abramov AY (2015) Mitochondrial Ca^{2+} in neurodegenerative disorders. *Pharmacol Res* 99:377–381.
27. Ghezzi D, et al. (2011) Mutations in TTC19 cause mitochondrial complex III deficiency and neurological impairment in humans and flies. *Nat Genet* 43(3):259–63.
28. Ziosi M, et al. (2017) Coenzyme Q deficiency causes impairment of the sulfide oxidation pathway. *EMBO Mol Med* 9(1):96–111.
29. Kruse SE, et al. (2008) Mice with Mitochondrial Complex I Deficiency Develop a Fatal Encephalomyopathy. *Cell Metab* 7(4):312–320.
30. Quintana A, Kruse SE, Kapur RP, Sanz E, Palmiter RD (2010) Complex I deficiency due to loss of Ndufs4 in the brain results in progressive encephalopathy resembling Leigh syndrome. *Proc Natl Acad Sci U S A* 107(24):10996–1001.
31. McQuibban GA, Lee JR, Zheng L, Juusola M, Freeman M (2006) Normal Mitochondrial Dynamics Requires Rhomboid-7 and Affects Drosophila Lifespan and Neuronal Function. *Curr Biol* 16(10):982–989.
32. Patterson VL, et al. (2014) Neural-specific deletion of HTRA2 causes cerebellar neurodegeneration and defective processing of mitochondrial OPA1. *PLoS One* 9(12):1–24.
33. Dooley J, Liston A (2012) Molecular control over thymic involution: From cytokines and microRNA to aging and adipose tissue. *Eur J Immunol* 42(5):1073–1079.
34. Savino W (2002) The thymus gland is a target in malnutrition. *Eur J Clin Nutr* 56:S46–S49.
35. Seksenyan A, et al. (2010) Thymic involution, a co-morbidity factor in amyotrophic lateral sclerosis. *J Cell Mol Med* 14(10):2470–2482.
36. Jeyaraju D V, Cisbani G, De Brito OM, Koonin E V, Pellegrini L (2009) Hax1 lacks BH modules and is peripherally associated to heavy membranes: implications for Omi/HtrA2 and PARL activity in the regulation of mitochondrial stress and apoptosis. *Cell Death Differ* 16(12):1622–1629.
37. Salviati L, et al. (2012) Haploinsufficiency of COQ4 causes coenzyme Q10deficiency. *J Med Genet* 49(3):187–191.
38. Alcázar-Fabra M, Navas P, Brea-Calvo G (2016) Coenzyme Q biosynthesis and its role in the respiratory chain structure. *Biochim Biophys Acta - Bioenerg* 1857(8):1073–1078.
39. Stefely JA, Pagliarini DJ (2017) Biochemistry of Mitochondrial Coenzyme Q Biosynthesis. *Trends Biochem Sci* 42(10):824–843.
40. Veling MT, et al. (2017) Multi-omic Mitoprotease Profiling Defines a Role for Oct1p in Coenzyme Q Production. *Mol Cell* 68(5):970–977.e11.
41. Kühl I, et al. (2017) Transcriptomic and proteomic landscape of mitochondrial dysfunction reveals secondary coenzyme Q deficiency in mammals. *Elife* 6:e30952.
42. Maltecca F, et al. (2015) Purkinje neuron Ca2+ influx reduction rescues ataxia in SCA28 model. *J Clin Invest* 125(1):263–274.